

# Stability of persistent currents in superfluid fermionic rings

Klejdja Khani,<sup>1,\*</sup> Andrea Barresi,<sup>2,†</sup> Marek Tylutki,<sup>2,‡</sup> Gabriel Wlazłowski,<sup>2,3,§</sup> and Piotr Magierski<sup>2,3,¶</sup>

<sup>1</sup>*Dipartimento di Fisica e Astronomia, Università di Bologna, Via Irnerio 46, 40127 Bologna, Italy*

<sup>2</sup>*Faculty of Physics, Warsaw University of Technology, Ulica Koszykowa 75, 00-662 Warsaw, Poland*

<sup>3</sup>*Department of Physics, University of Washington, Seattle, Washington 98195-1560, USA*

(Dated: June 17, 2024)

We investigate the stability of persistent currents in superfluid fermionic gases confined to a ring geometry. Our studies, conducted at zero temperature using time-dependent density functional theory, cover interaction regimes from strong (unitary Fermi gas) to weak (Bardeen-Cooper-Schrieffer regime) couplings. Stability is tested with respect to the presence of an external defect within the ring. The dissipation mechanism related to vortex generation is present in all interaction regimes. Interestingly, while the corresponding critical winding number is found to be independent of the regime, the flow energy dissipation and its origin strongly depend on it. Vortex emission is accompanied by Cooper pair breaking, which occurs even beyond the vortex core in the weakly interacting regime. The pair-breaking mechanism prevents the imprinting of a persistent current with a winding number above a threshold, which decreases as we approach the BCS regime. Our study reveals the existence of two types of critical winding numbers above which the currents cease to be persistent in Fermi superfluids: one related to the proliferation of quantum vortices and the other with the onset of the pair-breaking mechanism.

*Introduction.* — Persistent currents, the continuous flow of particles without dissipation in ring-shaped or similarly closed-loop traps, are fundamental phenomena that arise in quantum systems such as superfluids [1–3] or superconductors [4]. In the field of ultracold atomic physics, its study stands out as a pivotal area of research [5], promising a deep insight into quantum coherence and offering potential applications in quantum technologies [6, 7]. The requirement for a single-valued wave function means the phase change around the loop must be an integer multiple of  $2\pi$ , defining a series of meta-stable states corresponding to the (integer) winding numbers  $w$ , separated by energy barriers [1]. The loop within which the persistent current flows corresponds to the case of a constant winding number. However, if dissipative effects are present, we may also have transitions to lower circulation state values, like  $w \rightarrow w - 1$ . They can be induced by quantum/thermal phase slippage or by increasing the superfluid velocity beyond a certain critical value [8–14]. The dissipative effects vary depending on the nature of the superfluid. In condensed ultracold atoms of bosonic type, persistent current dissipation often arises from vortex proliferation within the superfluid, causing phase slippage and decay of the circulation [8, 9, 15, 16]. The stability of these currents has been extensively studied, both with and without external defects [8, 17–21]. In fermionic superfluids, the pair-breaking mechanism can significantly contribute to supercurrent dissipation [22], as seen in Josephson junctions experiments [23, 24]. Persistent currents in fermionic systems have been investigated theoretically [25, 26] and were only recently observed experimentally [9, 27]. In an experiment with ultracold atoms of  $^6\text{Li}$  [9], the effect of interaction strength on the critical winding number in the presence of external defects has been examined. These studies attributed the

dissipation of the current to vortex emission, finding that the gas tuned to a strongly interacting regime, referred to as a unitary Fermi gas (UFG), is particularly robust against the decay of the persistent currents, making it a very good candidate for applications in quantum sensing.

Despite these advancements, several questions about the dissipation mechanisms in ultracold Fermi systems of the persistent currents remain unanswered. Quantum vortices can be imaged in the experiments, and it is relatively easy to correlate their emergence with the current decay, which is not the case for the second possible mechanism of Cooper pair breaking. This leads to questions about the importance of the mechanisms as a function of the interaction strength, which is hard to establish directly from the experimental data. A crucial aspect is identifying the pair-breaking critical winding number ( $w_{pb}$ ), beyond which Cooper pair breaking becomes energetically favorable. Understanding the impact of unpaired particles or the normal component on the flow energy dissipation is crucial in the study of the stability of persistent currents. Furthermore, external factors such as defects or impurities can enhance Cooper pair breaking by acting as seed sites for pair-breaking events and promoting vortex emission. Comprehending the interplay between these factors is essential for predicting and controlling persistent currents in fermionic systems.

This theoretical study explores the time-dependent dynamics of fermionic persistent currents in a two-dimensional ring geometry, similar to the experimental setup of Ref. [9], across various interaction strengths from strong to weak attractive superfluid regimes. We focus on clarifying how the pair-breaking mechanisms, particularly relevant in the BCS regime [24], affect persistent current states and the flow energy. We investigate whether the presence of a normal component or

unpaired particles can induce transitions between metastable states and alter the energy landscape. Through a comprehensive analysis of both ground states and time-dependent evolutions of fermionic superfluids with imprinted currents, we identify two critical winding number values: the pair-breaking threshold ( $w_{pb}$ ) and the vortex emission threshold ( $w_c$ ).

*Theoretical model* — We study the persistent current dynamics at different interaction strengths, from the strongly interacting unitary limit, characterized by a diverging  $s$ -wave interaction strength, to a weakly attractive interacting superfluid known as the Bardeen-Cooper-Schrieffer regime. The superfluid dynamics is studied by means of density functional theory (DFT) techniques for superfluid Fermi gases [28–30]. In the computation, we use energy density functional known as the extended Superfluid Local Density Approximation (SLDAE) [31]. The static variant of this local DFT theory we apply here is formally equivalent to the mean-field Bogoliubov–de Gennes equations where the quasi-particles wavefunctions satisfy the equation

$$\mathcal{H}[\rho(\vec{r}), \nu(\vec{r})] \begin{pmatrix} u_n(\vec{r}) \\ v_n(\vec{r}) \end{pmatrix} = E_n \begin{pmatrix} u_n(\vec{r}) \\ v_n(\vec{r}) \end{pmatrix} \quad (1)$$

with  $(u_n(\vec{r}), v_n(\vec{r}))^T$  being the Bogoliubov amplitudes and  $E_n$  the quasiparticles states energy. The Hamiltonian  $\mathcal{H}[\rho, \nu]$  is a function of the normal  $\rho$  and anomalous  $\nu$  densities, defined as

$$\rho(\vec{r}) = 2 \sum_{E_n > 0} |v_n(\vec{r})|^2, \quad (2a)$$

$$\nu(\vec{r}) = \sum_{E_n > 0} u_n(\vec{r})v_n^*(\vec{r}), \quad (2b)$$

with the sum evaluated up to a cut-off energy  $E_c$  in order to take care of the ultraviolet divergence [28, 32]. We use the metric system, where  $m = \hbar = 1$ . The Hamiltonian has a generic form

$$\mathcal{H} = \begin{pmatrix} h(\vec{r}) - \mu & \Delta(\vec{r}) \\ \Delta^*(\vec{r}) & -h^*(\vec{r}) + \mu \end{pmatrix}, \quad (3)$$

where single particle Hamiltonian and pairing potentials are computed as appropriate functional derivatives of the energy functional  $\mathcal{E}$ , namely:

$$h = -\frac{1}{2}\nabla^2 + \frac{\delta\mathcal{E}}{\delta\rho} + V_{\text{ext}}(\vec{r}), \quad (4)$$

$$\Delta = -\frac{\delta\mathcal{E}}{\delta\nu^*}. \quad (5)$$

The chemical potential is denoted as  $\mu$ . The mean-field  $U = \delta\mathcal{E}/\delta\rho$  and pairing  $\Delta$  potentials are functions of the dimensionless coupling constant  $\lambda = a_s k_F$ , where  $a_s$  is the  $s$ -wave scattering length and  $k_F = (3\pi^2\rho)^{1/3}$  is the Fermi wave vector. The SLDAE description assures correct reproduction of the equation of state  $E(\lambda)$  and

strength of the pairing gap  $|\Delta(\lambda)|$ . For the explicit form of the energy functional  $\mathcal{E}$  and associated mean-fields, see Ref. [31].

The time-dependent framework is obtained by allowing Bogoliubov amplitudes to be time-dependent, i.e.  $u_n(\vec{r}, t)$  and  $v_n(\vec{r}, t)$ , which also makes the densities time-dependent quantities, and by replacing  $E_n \rightarrow i\frac{\partial}{\partial t}$  in Eq. (1). The model has been successfully applied to describe different physical phenomena such as the Josephson effect and dissipative mechanisms in a Josephson junction [24] or dissipative vortices dynamics [33–38], Higgs modes [39], properties of spin-imbalanced systems [29, 40–43] and even quantum turbulence [44–46].

In our setup the superfluid is trapped in a two-dimensional ring potential; see for visualization Fig. 1(c). The density is constant along the ring and goes to zero within a few coherence lengths at the edges. We impose translational symmetry along the  $z$ -direction, so the corresponding solutions are plane waves. We then imprint a phase  $\phi = w_0 \arctan(x, y)$  in the order parameter, so that  $\Delta(x, y) = |\Delta(x, y)|e^{i\phi}$ . In this way, a persistent current state corresponding to the winding number  $w_0$  is imprinted. Next, we study the stability of the persistent currents in the presence of a localized Gaussian defect by means of a time-dependent framework; see, for example, the inset of Fig. 3(a.i). The explicit form of the external potential is given in Appendix A.

Our studies are focused on three interaction regimes: unitary Fermi gas regime  $\lambda^{-1} \simeq 0$  (labeled hereafter as UFG), experimentally accessible regime  $\lambda^{-1} = -0.4$  (BCS limit) and  $\lambda^{-1} \simeq -1$ , which is presently inaccessible for experiments due to very low value of critical temperature (deep BCS or dBCS). The main quantity that we use to characterize the stability of the current is the flow energy

$$E_{\text{flow}}(t) = \int \frac{\vec{j}^2(\vec{r}, t)}{2\rho(\vec{r}, t)} d^3\vec{r}, \quad (6)$$

where

$$\vec{j}(\vec{r}) = 2 \sum_{E_n > 0} \text{Im} \left( v_n \vec{\nabla} v_n^* \right) = \rho(\vec{r}) \vec{v}(\vec{r}) \quad (7)$$

is the density current, which we also use to define velocity field  $\vec{v}$ . Note that, in general,  $\vec{v}$  is not the same as superfluid velocity  $\vec{v}_s = \frac{\hbar}{2m} \nabla \phi$ , since the framework accounts also for effects (like pair-breaking) that effectively lead to the emergence of a normal component. In the simulations, the total energy is conserved. However, the flow energy can change in time, indicating current decay if  $E_{\text{flow}}$  is decreasing. The next quantity that we extract throughout our studies is the condensation energy, defined as

$$E_{\text{cond}}(t) = \frac{3}{8} \int \frac{|\Delta(\vec{r}, t)|^2}{\varepsilon_F(\vec{r}, t)} \rho(\vec{r}, t) d^3\vec{r} \quad (8)$$

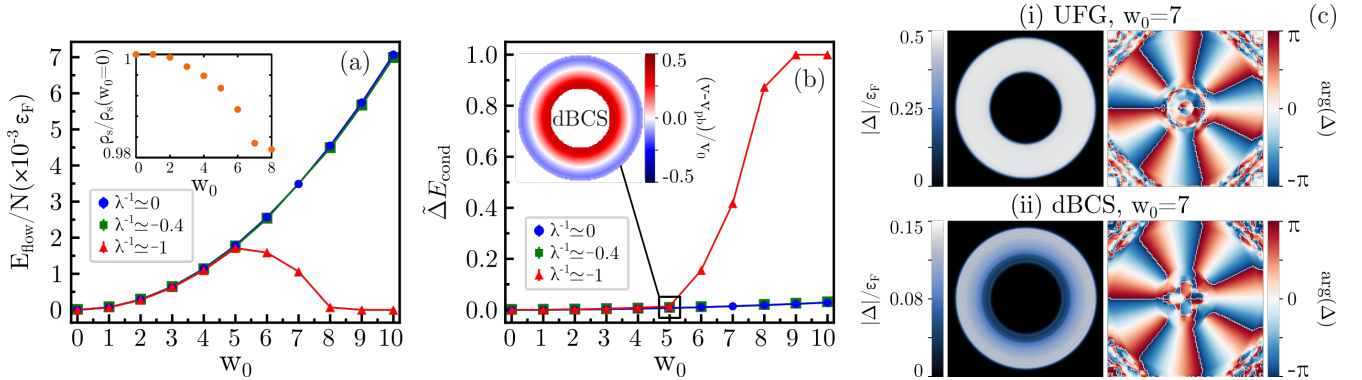


FIG. 1. Static calculations: The flow energy per particle number (a) and the relative condensation energy change  $\Delta E_{\text{cond}}$  (b) as a function of the imprinted winding number  $w_0$  from the UFG limit ( $\lambda^{-1} \simeq 0$ , blue dots) to deep-BCS ( $\lambda^{-1} \simeq -1$ , red triangles), with BCS ( $\lambda^{-1} \simeq -0.4$ , green squares) being an intermediate regime. The inset in (a) shows the bulk superfluid density at winding number  $w_0$  scaled to the corresponding value for  $w_0 = 0$ . The flow energy increases with  $w_0$  as  $E_{\text{flow}} \propto w_0^2$  in UFG and BCS limit for all  $w_0$  and for values of  $w_0 \leq w_{pb} = 5$  in dBCS regime as in the latter case the pair-breaking mechanism comes into play even in the absence of the defect. This occurs as the local velocity  $v$  exceeds the pair-breaking velocity  $v_{pb}$  at the ring's inner edge, as shown in the inset of (b), where  $v_0$  denotes the average value of the velocity in the ring. The pair-breaking mechanism becomes more effective when  $w_0$  is increased, eventually leading to a loss of superfluidity. The inset in (c) shows the absolute value of the order parameter and its phase in the  $xy$ -plane in UFG (i) and deep-BCS (ii) regimes. The two-dimensional phase plots correspond to the imprinted winding number  $w_0 = 7$ .

with  $\epsilon_F(\vec{r})$  being the local value of the Fermi energy [47]. It measures the amount of energy contained in the condensate of Cooper pairs and its decrease in time is a measure of the importance of pair-breaking mechanisms.

*Static calculations* — For each interaction regime, we perform a systematic study of the dependence of the flow and the condensation energy with respect to the initial winding number  $w_0$ , as shown in Fig. 1(a)-(b), respectively. Assuming that the system is a pure superfluid,  $\rho = \rho_s$ , (no broken Cooper pairs) and the velocity field is equivalent to the superfluid velocity,  $v = v_s$ , the flow energy reads

$$\begin{aligned} E_{\text{flow}} &= 2\pi L_z \int_{R_{\text{in}}}^{R_{\text{out}}} \frac{\rho_s(r) v_s^2(r)}{2} r dr \\ &= \frac{\pi L_z \rho_s w_0^2}{4} \ln(R_{\text{out}}/R_{\text{in}}), \end{aligned} \quad (9)$$

where  $R_{\text{in}}$ ,  $R_{\text{out}}$  are the inner and outer radius of the ring within which the density is constant, and  $L_z$  is the size of the system along the  $z$ -direction. The superfluid velocity induced by the imprinted phase profile is  $v_s(r) = w_0 \hbar / (2mr) = w_0 / 2r$  (in our units). Notably, as long as the flow is carried by superfluid fraction only, the flow energy remains independent of the interaction regime and scales as a square of the winding number  $w_0$ . This can be seen for UFG and BCS in the entire range of considered winding number values, while for dBCS simulations only for  $w_0 \leq 5$ , see Fig. 1(a). The departure from  $\sim w_0^2$  scaling above  $w_0 > 5$  is a clear signature of the breakdown of this assumption, as suggested by the inset of Fig. 1(a). In particular, the drop of  $E_{\text{flow}}$  to zero for  $w_0 \geq 9$  demonstrates that the imprinted phase no longer induces a flow – an unambiguous demonstration

that the system is in the normal state.

Further insight is provided by an analysis of the relative change of the condensation energy with respect to the state without imprinted current ( $w = 0$ ),  $\Delta E_{\text{cond}}(w_0) = \frac{|E_{\text{cond}}(w_0) - E_{\text{cond}}(w_0=0)|}{E_{\text{cond}}(w_0=0)}$ , see Fig. 1(b). A drop in the condensation energy signals the presence of a pair-breaking mechanism. In the UFG and BCS limits  $\Delta E_{\text{cond}}(w_0)$  increases slightly with  $w_0$ , remaining below 5% even at the highest explored value of  $w_0 = 10$ , which means that the pair-breaking mechanism is negligibly small. However, in the dBCS regime,  $\Delta E_{\text{cond}}$  rises rapidly above  $w_0 = 5$ , which allows us to introduce the critical winding number  $w_{pb}$  above which the broken pairs become essential contributions to the decay of a persistent current.

Next, we estimate the pair-breaking threshold  $v_{pb}$ , defined as [24, 48]

$$\tilde{v}_{pb} = \sqrt{\sqrt{\mu^2 + \Delta^2} - \mu^2}, \quad (10)$$

and compare it to the value of the local velocity  $v$ . As expected from the behavior of  $E_{\text{flow}}$ , for  $w_0 \geq 5$  in the dBCS regime,  $v$  surpasses the pair-breaking velocity, as shown in the inset of Fig. 1(b), where with blue (red) we show velocities below (above) the  $v_{pb}$ . Thus, we identify  $w_{pb} = 5$  as the *pair-breaking winding number* for the dBCS regime. Additionally, since the superfluid velocity decreases as  $1/r$ , the pair-breaking mechanism occurs first near the ring's inner edge,  $r = R_{\text{in}}$ . Consequently, for  $w_0 > w_{pb}$ , the order parameter  $|\Delta|$  reaches the lowest value at the inner edge of the ring, while in the UFG limit, it maintains a constant value across the ring diameter, as illustrated in Fig. 1(c) for  $w_0 = 7$ . As we increase  $w_0$ , the local velocity  $v$  exceeds  $v_{pb}$  even at a greater dis-

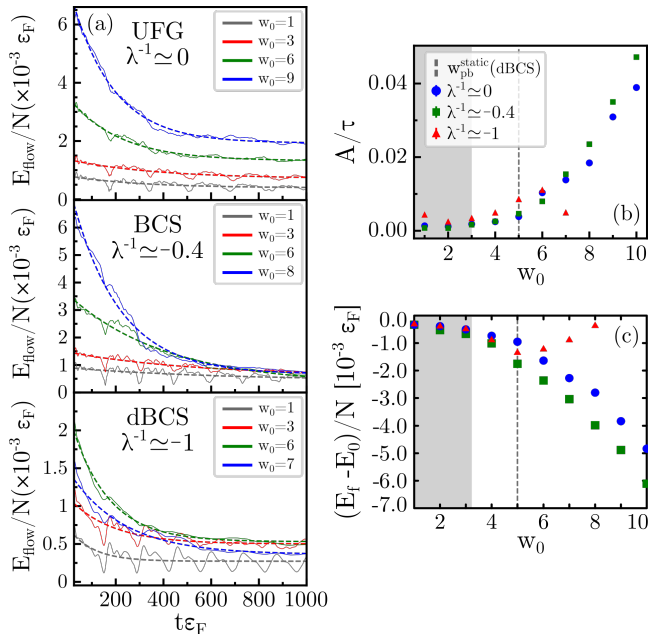


FIG. 2. Time-dependent calculations: (a) Temporal evolution of the flow energy for selected values of winding number  $w_0$  and for different interaction strengths  $\lambda^{-1}$  from UFG to dBCS limit, where the time is expressed in units of  $\epsilon_F$ . The dashed lines are the exponential fit  $F(t) = Ae^{-t/\tau} + B$ . (b,c) The dependence of the decay rate  $A/\tau$  and the energy loss  $E_f - E_0$  per particle as a function of winding number  $w_0$ . The shaded area indicates the values of the winding number for which there is only sound emitted due to the switch on the defect. The dashed line indicates the onset of pair-breaking phenomena in the deep-BCS regime extracted from the static considerations.

tance from the inner edge of the ring, and eventually, the superfluidity is completely lost.

*Dynamic calculations* — The static considerations demonstrated that the persistent currents can be affected significantly by Cooper pair breaking when a sufficiently large initial flow is imprinted. However, they do not provide information about stability of the currents once they are imprinted. To investigate this, we perform their time-dependent evolution. We study the stability in the defect's presence, as was done in experiment [9]. The defect's height is switched on until it reaches the final value  $V_0 \simeq 2\mu$  at  $t_0 = 25\epsilon_F^{-1}$ , having a  $1/e^2$  width of  $w = 10k_F^{-1}$ . The defect's parameters are kept fixed in all explored interaction regimes.

The stability is judged based on measurement of the temporal profile of the flow energy  $E_{\text{flow}}(t)$  after the defect is switched on, see Fig. 2(a). These data are fitted via an exponential function taken as

$$E_{\text{flow}}(t) = Ae^{-t/\tau} + B \quad (11)$$

where  $A$ ,  $B$  and  $\tau$  are fitting parameters with  $\tau$  the decay time. By taking the time derivative of Eq. (11) we note that  $A/\tau$  gives the decay rate of the flow energy, Fig. 2(b). Next, we define a second quantity named the

flow energy loss  $E_f - E_0$  with  $E_f = E_{\text{flow}}(t \rightarrow \infty)$  and  $E_0 = E_{\text{flow}}(t_0)$  being the final and initial flow energies respectively, Fig. 2(c). At low  $w_0$  values, the flow energy tends to remain relatively stable over time, with fluctuations due to turning on the defect procedure. However, as  $w_0$  increases, the decay rate  $A/\tau$  becomes larger, as illustrated in Fig. 2(b). Consequently, the amount of the energy loss also increases with  $w_0$  value, as depicted in Fig. 2(c). Interestingly, while we observe a similar trend in the dBCS case for  $w_0$  values up to  $w_0 = 5$ , flow energy dissipation decreases for even higher winding numbers, as we will discuss later. Furthermore, we find that dissipation in the BCS regime surpasses that in the UFG limit for equivalent  $w_0$  values. This observation suggests the presence of mechanisms that amplify dissipation specifically in the BCS regime. Consequently, we investigate the origins of dissipation in all three regimes and examine how it varies with initial winding number values.

Our analysis reveals two primary phenomena contributing to the dissipation of superflow energy: *generation of vortices* and/or *pair-breaking phenomena*. The former is revealed by the decay of the winding number in time: whenever a vortex is generated, it causes the phase slippage and removes one unit of the circulation. Thus, the instantaneous winding number (measured as a number of jumps of the phase by  $2\pi$  as we move along the inner edge of the ring) changes with steps, see Fig. 3(a). The latter contribution is instead discerned from the temporal behavior of the condensation energy, as illustrated in Fig. 3(b). Both phenomena lead to temporal changes in flow energy. An intriguing discovery is that the critical winding number  $w_c$ , denoted as the last value of  $w_0$  for which  $w(t) = w_0$ , appears to be independent of the interaction regime, consistently standing at the value of  $w_c = 2$ . However, we suspect this result may not be universally applicable and could vary depending on the defects' parameters. Notably, experimental investigations in Ref. [9], which featured defects considerably smaller than those in our study, reported  $w_c^{UFG} > w_c^{BCS}$ . In scenarios with weaker defects,  $w_c$  is anticipated to be higher [8] and could even exceeds  $w_{pb}$ .

For  $w_0 \geq 3$ , we observe the generation of quantum vortices. They are nucleated near the defect and may eventually propagate into the bulk, as shown in the insets of Fig. 3(a.i)-(a.ii) with 2D profiles of  $|\Delta|$  at selected moments and in Ref. [49]. Their number is related to  $(w(t) - w_0)$  value. Fig. 3(a.iii) shows the final winding number, extracted by an exponential fit of the  $w(t)$ , as a function of  $w_0$ . As  $w_0$  increases, the difference  $(w_0 - w_f)$  also increases, indicating the total amount of deposited vortices. For pure superfluid ( $\rho = \rho_s$ ), the flow energy is expected to be quadratically related to the winding number, so its decay in time clearly signals the energy loss. There is a striking feature of Fig. 3(a.iii) that requires clarification. There is no qualitative difference for  $(w_0 - w_f)$  when comparing different interaction regimes.

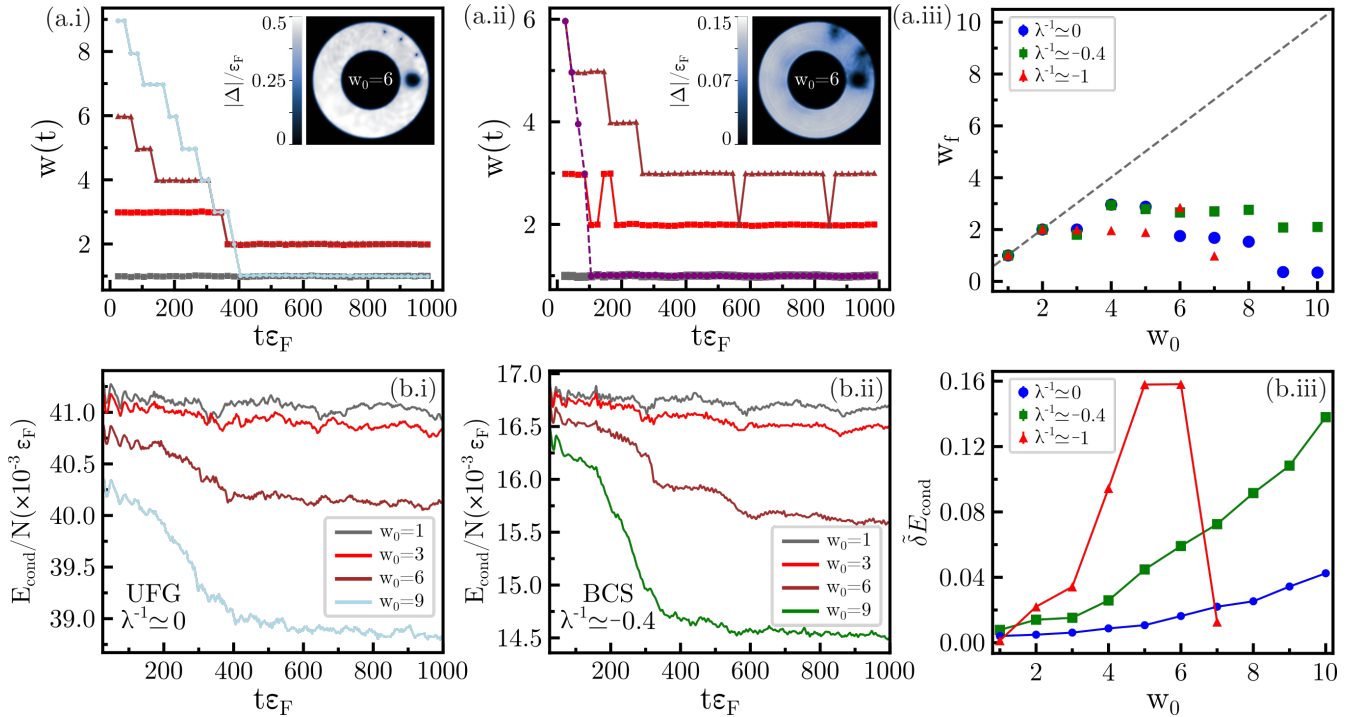


FIG. 3. The winding number, extracted at the ring's inner edge, as a function of time in UFG (a.i) and the dBCS regime (a.ii). The initial time  $t_0$  corresponds to the moment at which the height of the potential simulating the defect reaches its final value  $V_0/\mu \simeq 2$ . Insets: color maps of  $|\Delta(x, y)|/\varepsilon_F$  for  $w_0 = 6$  at times when several vortices propagate into the bulk in UFG and dBCS limit for  $t\varepsilon_F \simeq 430$  and  $t\varepsilon_F = 320$ , respectively. Subfigure (a.iii) shows final winding number  $w_f$  as a function of the initial winding number  $w_0$ , where  $w_f$  is extracted from the exponential fitting of  $w(t)$ . The dashed line indicates the ideal case where no phase-slippage events take place ( $w_f = w_0$ ). Condensation energy per particle as a function of time in UFG (b.i) and BCS regime (b.ii) for selected initial winding numbers. (b.iii) The difference in relative condensation energy change as a function of initial winding number for all three regimes (UFG, BCS, and dBCS).

At the quantitative level, the plot suggests that there are more vortices emitted and therefore expected enhanced dissipation in UFG regime as compared to BCS regime for  $w_0 > 6$  (green square points are systematically above blue dots). It is in tension with data presented in Fig 2(c), which points to the opposite.

To give further insight into this puzzling problem, we investigate the temporal behavior of our second observable: the condensation energy per particle  $E_{\text{cond}}(t)/N$ , shown in Fig. 3(b)-(i),(ii) for UFG and BCS limit. Given the scale differences between its values in different interaction regimes, we compare data by taking the normalized difference between final and initial values of  $E_{\text{cond}}$ :

$$\tilde{\delta}E_{\text{cond}} = \frac{E_{\text{cond}}(t_f) - E_{\text{cond}}(0)}{E_{\text{cond}}(0)}, \quad (12)$$

as illustrated in Fig. 3(b.iii) for all three regimes. The apparent difference in the condensation energy loss is clearly visible across different interaction regimes. Effectively, the loss can be interpreted as the production of the normal component at the cost of the flow energy. In general, this mechanism can operate independently. We may have a situation where the spatial distribution of the phase of the order parameter (and thus superfluid velocity  $v_s$ ) does not further change in time while part of the superfluid density is converted into normal density,

which dissipates the flow energy via viscosity. However, if quantum vortices are involved, one cannot decouple their generation from the pair-breaking. It is because of the peculiar structure of vortices in fermionic superfluids: the disruption of Cooper pairs in vortex cores is induced by velocities of the superflow exceeding the pair-breaking velocity (shown in Fig. 4(a)). When sufficient number of vortices are created, the portion of the superfluid volume in which  $|\Delta| \neq 0$  decreases, and  $E_{\text{cond}}$  follows suit. The drop of the condensation energy, as seen in Fig. 3(b.i) for UFG, is due to this process. The larger  $E_{\text{cond}}$  decrease for the dBCS regime is due to the larger vortex core size (inset fig. 3(a.ii)), but besides that, we also observe the pair-breaking process in action away from the defect and from the vortex cores, as demonstrated in Fig. 4(b). Figure 4(c) shows the systematic increase in the importance of the pair-breaking mechanics as we move from unitarity to BCS regimes.

In the deep BCS regime, for the large initial values of  $w_0$ , there is already a normal component (broken pairs) in the initial state, which significantly impacts the dynamics from the beginning. When  $w_0 > 6 > w_{pb}$ , the initial current state surpasses the pair-breaking critical velocity, leading to an initial partial loss of superfluidity. The latter promotes the emission of vortices during

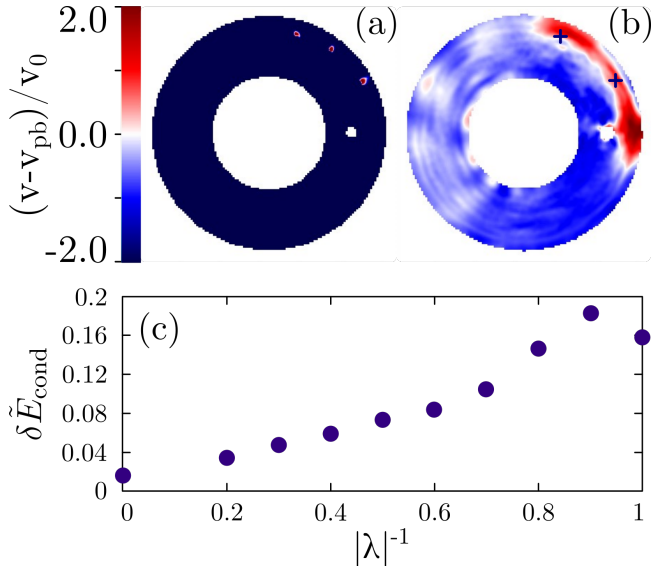


FIG. 4. (a) Velocity field with respect to pair-breaking velocity  $v(\vec{r}) - v_{pb}$  at unitarity ( $\lambda^{-1} \simeq 0$ ) at  $t\varepsilon_F \simeq 420$ . (b) Same quantity in dBCS regime ( $\lambda^{-1} \simeq -1$ ) at  $t\varepsilon_F \simeq 300$ . Crosses indicate vortex cores. (c) Difference in condensation energy (as defined in Eq. 12) as a function of  $|\lambda|^{-1}$  for a chosen value of imprinted winding number ( $w_0 = 6$ ).

the dynamics, even far from the defect region. For example, in the case of  $w_0 = 7$ , a vortex is emitted during the process of activating the defect. Therefore, the winding number at the time the defect is on, as shown in fig. 3(a.ii) is  $w(t_0) = 6$  instead of the imprinted value of  $w_0 = 7$ . Another consequence is the suppressed value of  $|\Delta|$ . Effectively, the coherence length  $\xi = \frac{k_F}{\pi\Delta}$  increases, which can even become comparable to the inner radius value. Thus, the inner hole can act as a larger additional defect from which vortices can be emitted while almost no further vortices are emitted close to the external defect, which now has a negligible width  $d \ll \xi$ . The decrease of  $|\Delta|$  at the static level lowers the initial flow and condensation energy value. This results in a higher value of  $E_f - E_0$  and lower  $\delta\tilde{E}_{\text{cond}}$ . If we further increase  $w_0$  we almost kill the superfluidity ( $\Delta \approx 0$ ), as it occurs for e.g. for  $w_0 = 8$ , and therefore  $\delta\tilde{E}_{\text{cond}}$  goes to zero. For  $w_0 = 9, 10$ , the initial state is composed of only the normal component, so we do not show these data in Fig. 3(b-iii). However, we must note that for  $w_0 > 8$ , as the time evolution proceeds, the system restores superfluidity, and  $E_{\text{cond}}$  increases in time; the superfluid fraction transits in a new equilibrium state. This new state is characterized by a non-zero  $w_f < w_0$  winding number.

*Conclusions* — Studying both static and dynamic fermionic ring superfluids reveals two distinct critical winding numbers. In the former scenario, the critical winding number ( $w_0 = w_{pb}$ ) is the point at which the local velocity surpasses the pair-breaking threshold, resulting in a decrease in the superfluid fraction. Notably, the pair-breaking critical winding number ( $w_{pb}$ ) is signif-

icantly lower in the deep BCS regime compared to the unitarity regime, aligning with expectations. As long as the amount of the normal component is marginal, the flow energy increases with  $w_0$  following a quadratic relationship. Transitioning towards the weakly attractive BCS limit, the breakup of Cooper-like pairs leads to a decline in both the superfluid fraction and the associated flow energy until superfluidity is lost.

The second critical winding number ( $w_c$ ) emerges in the presence of an external localized defect and represents the threshold for dynamic dissipation of the winding number caused by vortex generation. Notably,  $w_c$  remains unaffected by the interaction regime for our parameter choice. In particular, this study shows that the measurement of the winding number's decay is insufficient to decide if the current is persistent or decaying unambiguously. Here, we define the current as persistent if  $dE_{\text{flow}}/dt = 0$ . We identify situations where the flow energy decreases in certain time intervals, which is not reflected in the decay of  $w(t)$ . This is because the observables based solely on the winding number, while sensitive to the generation of quantum vortices, are only weakly sensitive to the broken pairs. We then explore the interplay between vortex emission and pair-breaking events during superfluid dynamics. Both of these phenomena directly impact flow energy dissipation, with the dissipation rate increasing with  $w_0$  and as we approach the BCS regime. Vortex emission notably influences the condensation energy due to the higher density of unpaired particles within the vortex cores, but broken pairs can also be produced independently from far away vortex cores and defects, which is particularly pronounced in the deep BCS regime. Conversely, preceding pair-breaking events before the external defect enhance the process of defect-induced vortex emission, as occurs in the deep BCS regime.

In the perspective of atomtronics applications and superconductors, further exploration could involve quantitative analysis of the dissipative phenomena discussed here in the presence of multiple defects along the superflow. The work also points to the importance of searching for another probe testing the stability of the superfluid flows, like probes that quantify superfluid fraction during the time evolution.

We are grateful to G. Roati, G. Del Pace, D. Peřak and B. Tüzemen for their insightful discussions and ideas. The calculations were executed by means of the W-SLDA Toolkit [50]. Reproducibility packs for restoration of results presented in this paper are available via Zenodo repository [49]. MT was supported by a National Science Centre grant UMO-2019/35/D/ST2/00201. AB, GW, and PM were supported by a National Science Centre grant UMO-2022/45/B/ST2/00358. This work used computational resources Tsubame3.0 supercomputer provided by Tokyo Institute of Technology through the HPCI System Research Project (Project

ID: hp230081). We also gratefully acknowledge Polish high-performance computing infrastructure PLGrid (HPC Centers: ACK Cyfronet AGH) for providing computer facilities and support within computational grant no. PLG/2024/016930 (p1ginhsf2).

## Appendix A: Shape of trapping potential and defect

The external potential is imprinted in an annular shape during the self-consistent procedure, defined by the following expression:

$$V_{\text{ext}}(\vec{r}) = \begin{cases} 2\varepsilon_F & r < R_{\text{in}} = 26k_F^{-1} \\ 2\varepsilon_F s(r - R_1^s, R_1^s - R_{\text{in}}) & R_{\text{in}} \leq r < R_1^s = 30k_F^{-1} \\ 0 & R_1^s \leq r < R_2^s = 56k_F^{-1} \\ 2\varepsilon_F s(r - R_2^s, R_{\text{out}} - R_2^s) & R_2^s \leq r < R_{\text{out}} = 60k_F^{-1} \\ 2\varepsilon_F & r \geq R_{\text{out}} \end{cases} \quad (13)$$

where  $s(a, A) = \frac{1}{2} + \frac{1}{2} \tanh[\tan[\frac{\pi}{2}(\frac{2a}{A} - 1)]]$  is a radial function that modifies the potential continuously between radii. This is done in order to prevent discontinuities, which would create numerical instabilities in the simulations. After the ground state has been determined, we dynamically raise an additional potential that models defect during the time-dependent part. The defect is placed at a position  $(x_D, y_D) = (\frac{R_{\text{out}} - R_{\text{in}}}{2}, 0)$  and is taken to have a Gaussian shape  $V(t) = f(t)V_0 e^{-2x_D^2/w^2} e^{-2y_D^2/w^2}$ , where the defect width is  $wk_F = 10$  and height  $V_0 = 2\mu$ . The function  $f(t)$  linearly rises from 0 to 1 in time interval  $t \in (0, t_0 = 25\varepsilon_F^{-1})$ , and for  $t > t_0$  is kept to be 1.

\* klejdja.xhani@unibo.it

† andrea.barresi.dokt@pw.edu.pl

‡ marek.tylutki@pw.edu.pl

§ gabriel.wlazlowski@pw.edu.pl

¶ piotr.magierski@pw.edu.pl

- [1] F. Bloch, "Superfluidity in a ring," *Phys. Rev. A* **7**, 2187–2191 (1973).
- [2] Erich J. Mueller, "Superfluidity and mean-field energy loops: Hysteretic behavior in bose-einstein condensates," *Phys. Rev. A* **66**, 063603 (2002).
- [3] A. J. Leggett, "Superfluidity," *Rev. Mod. Phys.* **71**, S318–S323 (1999).
- [4] Michael Tinkham, *Introduction to superconductivity* (Courier Corporation, 2004).
- [5] Changhyun Ryu, MF Andersen, Pierre Clade, Vasant Natarajan, Kristian Helmerson, and William D Phillips, "Observation of persistent flow of a bose-einstein condensate in a toroidal trap," *Physical Review Letters* **99**, 260401 (2007).
- [6] L. Amico, M. Boshier, G. Birkl, A. Minguzzi, C. Miniatura, L.-C. Kwek, D. Aghamalyan, V. Ahufinger, D. Anderson, N. Andrei, A. S. Arnold, M. Baker, T. A. Bell, T. Bland, J. P. Brantut, D. Cassettari, W. J. Chetcuti, F. Chevy, R. Citro, S. De Palo, R. Dumke, M. Ed-

wards, R. Folman, J. Fortagh, S. A. Gardiner, B. M. Garraway, G. Gauthier, A. Günther, T. Haug, C. Hufnagel, M. Keil, P. Ireland, M. Lebrat, W. Li, L. Longchambon, J. Mompert, O. Morsch, P. Naldesi, T. W. Neely, M. Olshani, E. Orignac, S. Pandey, A. Pérez-Obiol, H. Perrin, L. Piroli, J. Polo, A. L. Pritchard, N. P. Proukakis, C. Rylands, H. Rubinsztein-Dunlop, F. Scazza, S. Stringari, F. Tosto, A. Trombettoni, N. Victorin, W. von Klitzing, D. Wilkowski, K. Xhani, and A. Yakimenko, "Roadmap on atomtronics: State of the art and perspective," *AVS Quantum Science* **3**, 039201 (2021).

- [7] Luigi Amico, Dana Anderson, Malcolm Boshier, Jean-Philippe Brantut, Leong-Chuan Kwek, Anna Minguzzi, and Wolf von Klitzing, "Colloquium: Atomtronic circuits: From many-body physics to quantum technologies," *Rev. Mod. Phys.* **94**, 041001 (2022).
- [8] Klejdja Xhani, Giulia Del Pace, Francesco Scazza, and Giacomo Roati, "Decay of persistent currents in annular atomic superfluids," *Atoms* **11** (2023), 10.3390/atoms11080109.
- [9] G. Del Pace, K. Xhani, A. Muzi Falconi, M. Fedrizzi, N. Grani, D. Hernandez Rajkov, M. Inguscio, F. Scazza, W. J. Kwon, and G. Roati, "Imprinting persistent currents in tunable fermionic rings," *Physical Review X* **12** (2022), 10.1103/physrevx.12.041037.
- [10] Romain Dubessy, Thomas Liennard, Paolo Pedri, and H el ene Perrin, "Critical rotation of an annular superfluid bose-einstein condensate," *Physical Review A* **86**, 011602 (2012).
- [11] Juan Polo, Romain Dubessy, Paolo Pedri, H el ene Perrin, and Anna Minguzzi, "Oscillations and decay of superfluid currents in a one-dimensional bose gas on a ring," *Physical Review Letters* **123**, 195301 (2019).
- [12] Zain Mehdi, Ashton Bradley, Joseph Hope, and Stuart Szigeti, "Superflow decay in a toroidal bose gas: The effect of quantum and thermal fluctuations," *SciPost Physics* **11**, 080 (2021).
- [13] Masaya Kunimi and Ipppei Danshita, "Decay mechanisms of superflow of bose-einstein condensates in ring traps," *Physical Review A* **99**, 043613 (2019).
- [14] Laura Corman, Lauriane Chomaz, Tom Bienaim e, R emi Desbuquois, Christof Weitenberg, Sylvain Nascimbene, Jean Dalibard, and J er ome Beugnon, "Quench-induced supercurrents in an annular bose gas," *Physical review letters* **113**, 135302 (2014).
- [15] K. C. Wright, R. B. Blakestad, C. J. Lobb, W. D. Phillips, and G. K. Campbell, "Driving phase slips in a superfluid atom circuit with a rotating weak link," *Phys. Rev. Lett.* **110**, 025302 (2013).
- [16] Stuart Moulder, Scott Beattie, Robert P. Smith, Naaman Tammuz, and Zoran Hadzibabic, "Quantized supercurrent decay in an annular bose-einstein condensate," *Phys. Rev. A* **86**, 013629 (2012).
- [17] Avinash Kumar, Romain Dubessy, Thomas Badr, Camilla De Rossi, Mathieu de Go er de Herve, Laurent Longchambon, and H el ene Perrin, "Producing superfluid circulation states using phase imprinting," *Physical Review A* **97**, 043615 (2018).
- [18] Avinash Kumar, Stephen Eckel, Fred Jendrzejewski, and Gretchen K Campbell, "Temperature-induced decay of persistent currents in a superfluid ultracold gas," *Physical Review A* **95**, 021602 (2017).
- [19] Luca Pezz e, Klejdja Xhani, Cyprien Daix, Nicola Grani, Beatrice Donelli, Francesco Scazza, Diego Hernandez-

- Rajkov, Woo Jin Kwon, Giulia Del Pace, and Giacomo Roati, “Stabilizing persistent currents in an atomtronic josephson junction necklace,” (2023), [arXiv:2311.05523 \[cond-mat.quant-gas\]](https://arxiv.org/abs/2311.05523).
- [20] Stephen Eckel, Jeffrey G Lee, Fred Jendrzejewski, Noel Murray, Charles W Clark, Christopher J Lobb, William D Phillips, Mark Edwards, and Gretchen K Campbell, “Hysteresis in a quantized superfluid ‘atomtronic’ circuit,” *Nature* **506**, 200–203 (2014).
- [21] Scott Beattie, Stuart Moulder, Richard J Fletcher, and Zoran Hadzibabic, “Persistent currents in spinor condensates,” *Physical review letters* **110**, 025301 (2013).
- [22] Jee Woo Park, Bumsuk Ko, and Yong-il Shin, “Critical vortex shedding in a strongly interacting fermionic superfluid,” *Physical Review Letters* **121**, 225301 (2018).
- [23] A. Burchianti, F. Scazza, A. Amico, G. Valtolina, J. A. Seman, C. Fort, M. Zaccanti, M. Inguscio, and G. Roati, “Connecting dissipation and phase slips in a josephson junction between fermionic superfluids,” *Phys. Rev. Lett.* **120**, 025302 (2018).
- [24] Gabriel Wlazłowski, Klejdja Khani, Marek Tylutki, Nikolaos P. Proukakis, and Piotr Magierski, “Dissipation mechanisms in fermionic josephson junction,” *Phys. Rev. Lett.* **130**, 023003 (2023).
- [25] L. Pisani, V. Piselli, and G. Calvanese Strinati, “Critical current throughout the bcs-bec crossover with the inclusion of pairing fluctuations,” *Phys. Rev. A* **109**, 033306 (2024).
- [26] Giovanni Pecci, Piero Naldesi, Luigi Amico, and Anna Minguzzi, “Probing the bcs-bec crossover with persistent currents,” *Physical Review Research* **3**, L032064 (2021).
- [27] Yanping Cai, Daniel G Allman, Parth Sabharwal, and Kevin C Wright, “Persistent currents in rings of ultracold fermionic atoms,” *Physical Review Letters* **128**, 150401 (2022).
- [28] Aurel Bulgac, “Local-density-functional theory for superfluid fermionic systems: The unitary gas,” *Phys. Rev. A* **76**, 040502 (2007).
- [29] A. Bulgac and M.M. Forbes, “Unitary fermi supersolid: The larkin-ovchinnikov phase,” *Phys. Rev. Lett.* **101**, 215301 (2008).
- [30] Aurel Bulgac, Michael McNeil Forbes, and Piotr Magierski, “The Unitary Fermi Gas: From Monte Carlo to Density Functionals,” in *The BCS-BEC Crossover and the Unitary Fermi Gas*, Lecture Notes in Physics, edited by Wilhelm Zwerger (Springer, Berlin, Heidelberg, 2012) pp. 305–373.
- [31] Antoine Boulet, Gabriel Wlazłowski, and Piotr Magierski, “Local energy density functional for superfluid fermi gases from effective field theory,” *Physical Review A* **106**, 013306 (2022).
- [32] Aurel Bulgac and Yongle Yu, “Renormalization of the hartree-fock-bogoliubov equations in the case of a zero range pairing interaction,” *Phys. Rev. Lett.* **88**, 042504 (2002).
- [33] Andrea Barresi, Antoine Boulet, Piotr Magierski, and Gabriel Wlazłowski, “Dissipative dynamics of quantum vortices in fermionic superfluid,” *Phys. Rev. Lett.* **130**, 043001 (2023).
- [34] Aurel Bulgac, Yuan-Lung Luo, Piotr Magierski, Kenneth J. Roche, and Yongle Yu, “Real-time dynamics of quantized vortices in a unitary fermi superfluid,” *Science* **332**, 1288–1291 (2011).
- [35] Aurel Bulgac, Yuan-Lung Luo, and Kenneth J. Roche, “Quantum shock waves and domain walls in the real-time dynamics of a superfluid unitary fermi gas,” *Phys. Rev. Lett.* **108**, 150401 (2012).
- [36] Aurel Bulgac, Michael McNeil Forbes, Michelle M. Kelley, Kenneth J. Roche, and Gabriel Wlazłowski, “Quantized superfluid vortex rings in the unitary fermi gas,” *Phys. Rev. Lett.* **112**, 025301 (2014).
- [37] Gabriel Wlazłowski, Kazuyuki Sekizawa, Maciej Marchwiany, and Piotr Magierski, “Suppressed solitonic cascade in spin-imbalanced superfluid fermi gas,” *Phys. Rev. Lett.* **120**, 253002 (2018).
- [38] Marek Tylutki and Gabriel Wlazłowski, “Universal aspects of vortex reconections across the bcs-bec crossover,” *Phys. Rev. A* **103**, L051302 (2021).
- [39] Aurel Bulgac and Sukjin Yoon, “Large amplitude dynamics of the pairing correlations in a unitary fermi gas,” *Phys. Rev. Lett.* **102**, 085302 (2009).
- [40] Aurel Bulgac, Michael McNeil Forbes, and Achim Schwenk, “Induced  $p$ -wave superfluidity in asymmetric fermi gases,” *Phys. Rev. Lett.* **97**, 020402 (2006).
- [41] Jakub Kopyciński, Wojciech R. Pudelko, and Gabriel Wlazłowski, “Vortex lattice in spin-imbalanced unitary fermi gas,” *Phys. Rev. A* **104**, 053322 (2021).
- [42] Piotr Magierski, Buğra Tüzemen, and Gabriel Wlazłowski, “Spin-polarized droplets in the unitary fermi gas,” *Phys. Rev. A* **100**, 033613 (2019).
- [43] Piotr Magierski, Buğra Tüzemen, and Gabriel Wlazłowski, “Dynamics of spin-polarized impurity in ultracold fermi gas,” *Phys. Rev. A* **104**, 033304 (2021).
- [44] Gabriel Wlazłowski, Aurel Bulgac, Michael McNeil Forbes, and Kenneth J. Roche, “Life cycle of superfluid vortices and quantum turbulence in the unitary fermi gas,” *Phys. Rev. A* **91**, 031602 (2015).
- [45] Khalid Hossain, Konrad Kobuszewski, Michael McNeil Forbes, Piotr Magierski, Kazuyuki Sekizawa, and Gabriel Wlazłowski, “Rotating quantum turbulence in the unitary fermi gas,” *Phys. Rev. A* **105**, 013304 (2022).
- [46] G. Wlazłowski, M. M. Forbes, S. R. Sarkar, A. Marek, and M. Szpindler, “Fermionic quantum turbulence: Pushing the limits of high-performance computing,” *PNAS Nexus* **3**, 160 (2024).
- [47] Gabriel Wlazłowski, Klejdja Khani, Marek Tylutki, Nikolaos P. Proukakis, and Piotr Magierski, “Dissipation mechanisms in fermionic josephson junction,” *Physical Review Letters* **130**, 023003 (2023).
- [48] A. Spuntarelli, P. Pieri, and G.C. Strinati, “Solution of the bogoliubov–de gennes equations at zero temperature throughout the BCS–BEC crossover: Josephson and related effects,” *Physics Reports* **488**, 111–167 (2010).
- [49] Klejdja Khani, Andrea Barresi, Marek Tylutki, Gabriel Wlazłowski, and Piotr Magierski, “Stability of persistent currents in superfluid fermionic rings: Supplementary material,” (2024), available at <https://zenodo.org/records/11526086>.
- [50] “W-SLDA Toolkit,” <https://wsllda.fizyka.pw.edu.pl/>.